International Journal of Heat and Mass Transfer 154 (2020) 119704

Contents lists available at ScienceDirect

International Journal of Heat and Mass Transfer

journal homepage: www.elsevier.com/locate/hmt

Numerical analysis of heat and mass transfer in kiwifruit slices during combined radio frequency and vacuum drying

Lixia Hou[a], Xu Zhou[b], Shaojin Wang[a,b,*]

[a] College of Mechanical and Electronic Engineering, Northwest A&F University, Yangling, Shaanxi 712100, China
[b] Department of Biological Systems Engineering, Washington State University, 213 L.J. Smith Hall, Pullman, WA 99164-6120, USA

ARTICLE INFO

Article history:
Received 21 January 2020
Revised 21 March 2020
Accepted 25 March 2020
Available online 17 April 2020

Keywords:
Kiwifruit
Heat-mass transfer
Shrinkage
RF-vacuum
Drying

ABSTRACT

Kiwifruit slices subjected to combined radio frequency (RF) and vacuum drying undergo a complicated process, including electromagnetic heating, heat and mass transfer along with a phase change of evaporation and shrinkage under a low pressure. The aim of this paper was to obtain an in-depth understanding of this complicated drying process. A 3D multiphase porous model was established to describe heat and mass transfer within the kiwifruit slices in a 3 kW, 27.12 MHz RF-vacuum drying system using COMSOL Multiphysics software. The validation results showed that the established model could be applied to describe the RF-vacuum drying process of kiwifruit slices since the maximum relative errors of temperature, moisture content, and drying rate between simulation and experiment were less than 10%. The temperature distribution of kiwifruit slices both from simulation and experiment indicated that the sample temperature at corners and edges were higher than that at the center of the container, and the sample temperature at the center was the lowest for a single kiwifruit slice. But the distribution of moisture content was opposite to that of temperature. Evaporation rate constant was found to be sensitive to moisture content of treated samples compared with temperature. The influences of sample thickness, electrode gap, and vacuum pressure of the RF-vacuum drying system on temperature and moisture content-time histories were determined during the RF-vacuum drying process. The findings of this research may help to gain a comprehensive understanding of RF-vacuum drying and optimize treatment parameters for drying processes.

1. Introduction

Kiwifruit (*Actinidia deliciosa*) is a commercial fruit of China, Chile, Greece, and New Zealand for high amount of antioxidant activity, flavonoids, phenols, and vitamin C [1]. It is considered as an obvious seasonal and regional fruit harvested from September to October in China. Due to its high-water content (above 80% wet basis), kiwifruit has a very short shelf/storage life even though it is kept in a cold storage. Therefore, it is necessary to use various methods to improve its shelf/storage life. Drying is a widely used method in food industry to extend the shelf/storage life of fresh products, such as fruits and vegetables, by removing a certain amount of water, and thus minimizing the spoilage caused by microbial growth. Furthermore, drying can save cost of transportation and storage for lighter weight and less space, and avoiding the need of expensive refrigeration systems with the operational cost.

Various drying methods were used to reduce water content from kiwifruit, such as hot air [2], freeze [3], osmotic [4], solar energy [5], and vacuum dehydration [2]. However, the main disadvantages of hot-air drying methods are high energy consumption, low efficiency, lengthy drying time, and low product quality [2,6]. Freeze drying and vacuum dehydration are considered as high running cost methods owing to the high energy consumption to maintain low temperature or pressure during the whole drying process [6]. It is reported that osmotic drying is not enough to reduce moisture contents of food to an acceptable level for low solute concentrations even when undergoing a long dehydration process [4]. Although solar energy drying is an environment friendly drying method, it takes long drying processes for high moisture content samples and is also limited by the local weather conditions. In recent years, radio frequency (RF) energy has been investigated as a new drying method for fruits and vegetables due to its fast and volumetric heating [7,8]. To minimize the quality loss of treated samples caused by non-uniform heating, RF energy has been used

* Corresponding author at: College of Mechanical and Electronic Engineering, Northwest A&F University, Yangling, Shaanxi 712100, China
E-mail addresses: shaojinwang@nwsuaf.edu.cn, shaojin_wang@wsu.edu (S. Wang).

https://doi.org/10.1016/j.ijheatmasstransfer.2020.119704
0017-9310/

Nomenclature

C_w	concentration (mol/m^3)
C_i	specific heat (J/(kg·K))
D_i	diffusion coefficient (m^2/s)
DR	drying rate (mol/(m^3 min))
E	electric field intensity (V/m)
f	frequency (Hz)
h_m	mass transfer coefficient (m/s)
h_t	heat transfer coefficient (W/(m^2 K))
I	rate of evaporation (kg/(m^3 s))
k	thermal conductivity (W/(m K))
K_{vap}	evaporation rate constant (1/s)
m_i	weight (g)
M	moisture content (dry basis)
M_w	molecular weight (kg/mol)
$n_{i,sur}$	boundary flux (mol/(m^2 s))
P^*	equilibrium vapor pressure (Pa)
P_G	vacuum pressure (Pa)
q_n	outward normal heat flux (W/m^2)
Q	RF power conversed to thermal energy (W/m^3)
R_w	reaction term (mol/(m^3 s))
S_i	saturation of fluid phase (dimensionless)
T_i	temperature (°C)
t	time (s)
u	convective velocity (m/s)
v_i	velocity (m/s)
V	voltage (V)
V_i	volume (m^3)
Δt	time interval (min)

Greek symbols

σ	electrical conductivity (S/m)
ρ_i	density (kg/m^3)
λ	latent heat of vaporization (J/kg)
ω_a, ω_v	mass fraction of air and vapor
ϕ	porosity (dimensionless)
ε_0	free space permittivity (8.86 × 10^{-12} F/m)
ε'	dielectric constant (dimensionless)
ε''	dielectric loss factor (dimensionless)
ε_{hs}	hygroscopic swelling strain (dimensionless)
β_h	coefficient of hygroscopic swelling (m^3/kg)
∇	gradient operator

Subscripts

a	air
g	gas
s	solid
t	total
v	vapor
w	water
eff	effective

in combination with traditional drying methods, such as hot air-assisted RF drying [9-11] and RF-vacuum drying [12-14]. Compared with hot air-assisted RF drying, the sensory and nutritive qualities of RF-vacuum treated sample are effectively maintained due to the relatively short drying time and low drying temperature [12].

RF-vacuum drying of kiwifruits is a complicated process, which involves electromagnetic heating, heat and mass transfer, phase change of evaporation, and shrinkage in a multiphase porous sample under the low pressure. Comparing with experimental method, computer simulation is a cheap, flexible, and visual method to realize this complicated drying process. Up to now, numerous researches on computer simulation have been conducted on improving RF heating uniformity [15-21], and predicting evaporation rate [22] and mass transfer [23] of the vacuum drying. Verified computer models have been established to determine effects of electrode gaps [24], forced air [24,25], sample moving [24], package geometries [25], and surrounding materials [16,18,21] on improving the RF heating uniformity. However, these models are established without considering water loss of samples. The dynamic characteristics of the vacuum drying, such as distributions of pressure, temperature, evaporation rate, and liquid holdup, have been analyzed by a validated model of vacuum drying [22]. Furthermore, a thin layer model has been used to analyze mass transfer properties using Fick's equation of diffusion and thermodynamic parameters of apple slices heated at 50, 60, and 70 °C under 0.02 bar [23]. To the author's knowledge, there is few literature on RF-vacuum drying models to explain this complicated drying process. Therefore, it is necessary to establish a 3-D model for better analyzing the factors influencing drying rate, temperature distribution, and shrinkage during the whole RF-vacuum drying process.

The main objectives of this paper were: (1) to establish a 3-D mathematical model for RF-vacuum drying based on twenty-four kiwifruit slices using a finite element software COMSOL, (2) to verify the model by comparing with the experimental temperature, moisture content, and drying rate of kiwifruit slices during RF-vacuum drying from a previous study, (3) to conduct a sensitivity analysis of input parameters affected the moisture content and temperature of treated samples, and (4) to apply the validated model for evaluating influences of the main factors on drying characteristics of kiwifruit slices during RF-vacuum drying.

2. Material and methods

2.1. Model development

In this section, a porous medium with multiphase and multicomponent coupled with shrinkage of inelastic sold matrix was presented to describe drying performances of kiwifruit slices during RF-vacuum treatments. The following assumptions were made to simplify the RF-vacuum drying process: (1) the RF system was assumed to operate at a constant top electrode voltage, (2) the temperature of air in the RF cavity was assumed to be constant during the RF heating process, (3) the three fluid phases (solid, liquid water and gas) were in continuum, (4) gas pressure was shared by all fluid phases, (5) thermal equilibrium existed between all phases, (6) kiwifruit slices were assumed to be a homogenous and isotropic material, and (7) thermal expansion of kiwifruit slices during drying was ignored. Governing equations, mass and energy conservation, initial and boundary conditions were described below.

2.1.1. Governing equations

The electric field intensity in the RF cavity was calculated by Maxwell's equations. Since the wavelength (11 m) in the 27.12 MHz RF system was far longer than the size of RF cavity (diameter: 0.8 m, length: 0.8 m) used in this study, the Maxwell's equation could be simplified to the Laplace equation by neglecting the effect of magnetic fields. The Laplace equation was described below using a quasi-static assumption [26]:

$$-\nabla \cdot ((\sigma + j2\pi f \varepsilon_0 \varepsilon')\nabla V) = 0 \quad (1)$$

where σ means electrical conductivity of the kiwifruit or air (S/m) and f delegates the frequency (Hz) of the RF system, $\varepsilon_0$is the permittivity of free space (8.86 × 10^{-12} F/m) while ε' represents dielectric constant of kiwifruit slices or air, j=$\sqrt{-1}$, and V refers to the voltage (V) between the two electrodes involved in the electric field intensity. Then, the electric field intensity (E) could be written

as the following equation:

$$E = -\nabla V \tag{2}$$

When the kiwifruit slices were placed between the two RF electrodes, which are under electromagnetic fields, the RF power (Q, W/m^3) absorbed in the dielectric material could be expressed as [27]:

$$Q = 2\pi f \varepsilon_0 \varepsilon'' \left|\vec{E}\right|^2 \tag{3}$$

where ε'' means the loss factor of kiwifruit. The heat conduction equation was taken place within the kiwifruit, heat convection at the sample's surface and heat generation in the kiwifruits due to RF energy. The heat transfer inside the heated kiwifruit is described by Fourier's equation [28]:

$$\rho C_p \frac{\partial T}{\partial t} = \nabla \cdot (k \nabla T) + Q \tag{4}$$

where C_p and ρ are the specific heat (J/(kg·K)) and density (kg/m^3) of kiwifruit, respectively.$\partial T/\partial t$ is the heating rate in samples (°C/s), k is the thermal conductivity (W/(m·K)), and T is the temperature (°C) of kiwifruit slices in the electromagnetic fields. The heat energy in the kiwifruits transferred from electromagnetic fields and transport in porous media was analyzed based on the electric currents and heat transfer in porous media module using finite element software COMSOL 5.2a Multiphysics (COMSOL Inc., Shanghai, China).

2.1.2. Mass conservation

The kiwifruit slices might be considered as mixture of the solid phase of kiwifruit, the liquid phase of water, and the gas phase of water vapor and air. The transports of components (liquid water, water vapor, and air) in kiwifruits during the RF-vacuum drying were simulated by a multiphase porous media model. For a volume element, porosity (ϕ, dimensionless) was expressed as a ratio of pores volume occupied by liquid water, water vapor, and air to the total volume of gas, liquid water and solid phase, and given by the following equation [29]:

$$\phi = \frac{\Delta V_g + \Delta V_w}{\Delta V_t} \tag{5}$$

where ΔV_w and ΔV_g are the volumes occupied by liquid water (m^3) and gas (including water vapor and air) (m^3), respectively. ΔV_t is the total volume of kiwifruits containing solid phase, liquid water, water vapor, and air (m^3).

For the pores in an elemental volume, water saturation (S_w, dimensionless) and gas saturation (S_g, dimensionless) are defined as a ratio of the volume of liquid water or gas to the total volume of pores [30]:

$$S_w = \frac{\Delta V_w}{\Delta V_g + \Delta V_w} \tag{6}$$

$$S_g = \frac{\Delta V_g}{\Delta V_g + \Delta V_w} = 1 - S_w \tag{7}$$

The concentration of liquid water (C_w, mol/m^3) is calculated by the mass conservation equation, including the convection term, diffusion term, and reaction term (phase change) [31]:

$$\frac{\partial C_w}{\partial t} + \nabla \cdot (-D_w \cdot \nabla C_w) + u \cdot \nabla C_w = -R_w \tag{8}$$

where D_w is the diffusion coefficient of species (m^2/s). u means the convective velocity of water (m/s). R_w delegates the reaction rate (mol/(m^3·s)) describing the production or consumption of water that was calculated and discussed in the following section. This was simulated in COMSOL using the transport module of diluted species.

2.1.3. Liquid phase evaporation

The evaporation rate (I, kg/(m^3·s)) is related to the equilibrium vapor pressure (p^*, Pa) of gas in the sample, the vacuum pressure (p_G, Pa), and the density of liquid water. The evaporation rate was equal to zero when the concentration of liquid water was less than zero or the equilibrium vapor pressure was smaller than the vapor phase pressure. If the concentration of liquid water was greater than zero, the evaporation rate can be expressed as [32]:

$$I = K_{vap} \rho_L (p* - p_G)/p_G \tag{9}$$

where K_{vap} is the evaporation rate constant (1/s) and ρ_L is the density of liquid phase (kg/m^3). Due to the assumption of zero resistance to vapor phase mass transfer in the present model, the vapor phase pressure would be constant and equal to the vacuum pressure in all points of the sample before the drying process. The equilibrium vapor pressure of gas in the sample can be evaluated from the Antoine equation [33]:

$$p* = 10^{A-B/(C+T)} \tag{10}$$

The parameters of A, B, and C were constant during vacuum drying [34]. Drying rate (DR.) was expressed as:

$$DR = \frac{M_i - M_{i-1}}{\Delta t} \tag{11}$$

where M_i or M_{i-1} is the moisture content of treated samples at any time i or *i-1*, and Δt is drying time interval between time i and *i-1* (min).

2.1.4. Energy conservation

The three phases in kiwifruits, including solid phase of kiwifruits, liquid phase of water, and gas phase of water vapor and air, were supposed to be in heat balance and shared the same energy balance equation. Energy conservation includes heat conduction, convection of fluid phases, evaporative cooling and the RF heat source term is described below [35]:

$$\rho_{eff} C_{eff} \frac{\partial T}{\partial t} + \sum_{i=w,v,a} (\rho_i C_{p,i} u_i \nabla T) = \nabla (k_{eff} \nabla T) - \lambda I + Q \tag{12}$$

The evaporation rate, I, and RF heat absorption, Q, of treated samples are related to location and time. λ is the latent heat of vaporization (J/kg). The properties of the mixture, ρ_{eff}, C_{eff}, and k_{eff}, were calculated by the properties of pure components and their mass or volume ratios [30]:

$$\rho_{\text{eff}} = (1-\varphi)\rho_s + \varphi(S_w \rho_w + S_g \rho_g) \tag{13}$$

$$C_{eff} = m_s C_{p,s} + m_w C_{p,w} + m_g(\omega_a C_{p,a} + \omega_v C_{p,v}) \tag{14}$$

$$k_{eff} = (1-\varphi)k_s + \varphi(S_w k_w + S_g(\omega_v k_v + \omega_a k_a) \tag{15}$$

where ω_a and ω_v represent mass fraction of air and vapor, respectively. m_s, m_w, and m_g are weight (kg) of solid, water, and gas in kiwifruit, respectively. This was implemented in COMSOL using the heat transfer in porous media module.

2.1.5. Determination of the amount of shrinkage in the dried samples

During the RF-vacuum drying process, the RF heating causes moisture transport from the inside of kiwifruit slices to the surface, where evaporation takes place. The evaporation and loss of moisture may cause the kiwifruit shrinkage, and change the drying stresses and strains during the RF-vacuum drying process. Therefore, the shrinkage analysis can be conducted after the solution of heat/mass transfer model. Through further analysis of heat and mass transfer simulation results, the drying shrinkage-deformation of kiwifruits versus time was obtained. According to the inelastic strain theory, the hygroscopic swelling strain (ε_{hs}) of kiwifruits

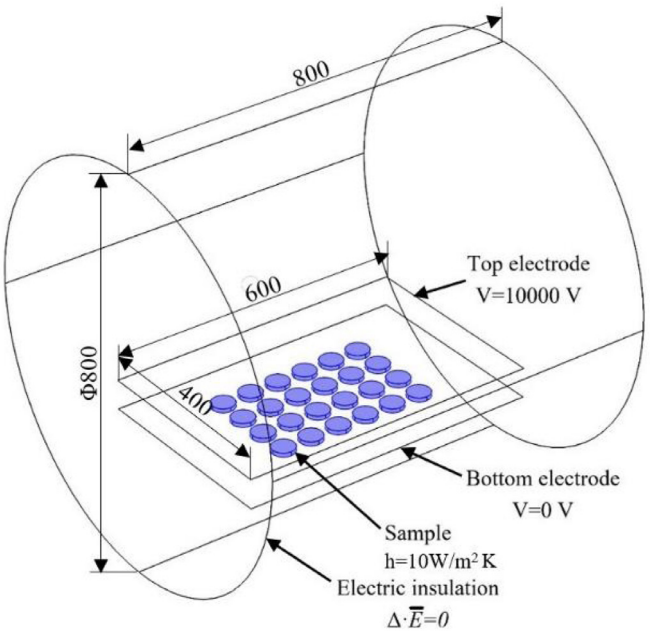

Fig. 1. Three-dimensional scheme of the RF-vacuum drying system with kiwifruit samples.

during the RF-vacuum drying could be calculated using the following equation [36] and was implemented in COMSOL using the solid mechanics module:

$$\varepsilon_{hs} = \beta_h M_w (C_w - C_{w,ref}) \tag{16}$$

where β_h is coefficient of hygroscopic swelling (m^3/kg) and $C_{w,ref}$ is initial concentration of liquid water during drying process. M_w is the molecular weight of water (kg/mol).

2.1.6. Initial and boundary conditions in the established model

The electrical, geometrical, and thermal boundary conditions of the RF-vacuum system applied in the simulation model are provided in Fig. 1. The voltage of the top electrode was set as 10,000 V, which was evaluated by matching the calculated results with experimental values of heating temperature and evaporation rate of the treated sample [26]. The bottom electrode and the metallic enclosure were set as ground. The boundary conditions of the electromagnetic field were considered as perfect conductors at the RF cavity walls and defined as electrical insulation ($\nabla E = 0$). The initial moisture content of sample and initial pressure in the RF cavity were uniform and listed in Table 1.

Data of dielectric and thermal properties of kiwifruit are necessary in modeling the RF-vacuum drying process. The dielectric constant and loss factor of kiwifruit changed with temperature (T, °C) and moisture content (M, d.b.) of the samples and can be expressed as following equations [14]:

$$\begin{aligned}\varepsilon_s' &= 38.08 + 0.83 \times T - 171.83 \times M - 0.98 \times T \times M - 1.71 \times 10^{-3} \\ &\times T^2 + 668.96 \times M^2 \\ &- 0.65 \times 10^{-3} \times M \times T^2 + 0.49 \times M^2 \times T + 3.37 \times 10^{-5} \\ &\times T^3 - 448.91 \times M^3\end{aligned} \tag{17}$$

$$\begin{aligned}\varepsilon_s'' &= -231.28 + 0.05 \times T - 1405.36 \times M + 1.08 \times M \times T \\ &+ 0.06 \times T^2 - 804.01 \times M^2 \\ &- 6.13 \times 10^{-6} \times T^2 + 1.77 \times 10^{-3} \times T - 804.01 \times M^2\end{aligned} \tag{18}$$

Since thermal properties of samples decided mostly by composition, heat capacity and thermal conductivity can be computed based on the composition of kiwifruit [37]. According to the literatures [38], moisture content, carbohydrate, protein, ash, and fat of kiwifruit were 84.0%, 10.5%, 1.0%, 0.7%, and 0.5%, respectively. The thermal conductivity (k) and specific heat (C_p) of kiwifruits can be computed as follows [37].

$$\begin{aligned}C_p &= 0.84 \times C_{pwater} + 0.105 \times C_{pCHO} + 0.01 \\ &\times C_{pprotein} + 0.007 \times C_{pash} + 0.005 \times C_{pfat} \\ &= 3700.6 + 0.1502 \times T + 3.9101 \times 10^{-3} \times T^2\end{aligned} \tag{19}$$

$$\begin{aligned}k &= 0.84 \times k_{water} + 0.105 \times k_{CHO} + 0.01 \times k_{protein} \\ &+ 0.007 \times k_{ash} + 0.005 \times k_{fat} \\ &= 0.5935 + 1.7693 \times 10^{-3} \times T - 6.1282 \times 10^{-6} \times T^2\end{aligned} \tag{20}$$

Water vapor flux ($n_{v,sur}$, mol/(m^2 s)) generated within the sample domain could move out from the sample by convection and diffusion, and was given as a boundary condition (Eq. (21)) on the surface of the sample. Liquid water flux ($n_{w,sur}$, mol/(m^2 s)) could move out from the boundary (Eq. (22)) as vapor after evaporation [46].

$$n_{v,sur} = C_v v_{n,v} + h_m \varphi S_g (\rho_v - \rho_{v,amb}) / M_w \tag{21}$$

$$n_{w,sur} = h_m \varphi S_w (\rho_v - \rho_{v,amb}) / M_w \tag{22}$$

where $v_{n,v}$ is the vapor velocity (m/s) on the sample boundaries. h_m is the mass transfer coefficient (m/s). ρ_v is the vapor density on the sample surface (kg/m^3). $\rho_{v,\,amb}$ is the vapor density in ambient air (kg/m^3).

Along with the mass flux of the vapor, the sample boundaries also lose heat (Eq. (23)) because of the lost vapor, and cooling by convection at room temperature in the air domain [46].

$$q_n = n_{v,sur} C_{p,v} T M_w + n_{w,sur} (\lambda + C_{p,v} T) + h_t (T - T_a) \tag{23}$$

where q_n is the outward normal heat flux (W/m^2), h_t is the convective heat transfer coefficient (W/(m^2 K)), and T_a is the ambient air temperature (K).

The diffusion coefficient of water in kiwifruit was calculated by the following equation [41]:

$$D_w = 1 \times 10^{-8} \cdot \exp(-2.8 + 2 \cdot M_w) \tag{24}$$

2.1.7. Process of computer simulations

A finite element analysis software, COMSOL, was used to simulate the heat and mass transfer during the RF-vacuum drying. The electric currents and heat transfer in porous media module were firstly solved to obtain the heat energy in the kiwifruits transferred from electromagnetic fields and then the temperature distribution of kiwifruit. Then, the moisture gradient was obtained from mass transfer using the transport module of diluted species. After that, the hygroscopic swelling strain distribution of kiwifruit slices was obtained using the solid mechanics module. All the main parameters needed in this paper were obtained by testing or reviewing relevant literatures. According to the accepted accuracy with the relatively low resource consumption, extra finer mesh was used and consisted of 531,012 domain elements (tetrahedral) used in subsequent simulation runs. Times of 1 and 5 min were used as the initial and maximum steps, respectively. The software was run on a 1.7 GHz Windows Lenovo workstation with an Intel Xeon CPU E5-2609, 1.70 GHz, 64 GB RAM on a windows 10 64 bit operating system for a total running time of 1020 min.

2.2. Model validation

To validate the established model, the simulated results were compared with the experimental values obtained from the previous study [13]. The thickness of kiwifruit slices was 8.0 ± 0.2 mm

Table 1
Physical parameters of kiwifruit used in the simulations.

Parameters	Symbols	Values	Units	References
Electromagnetics				
Radio frequency	f	27.12	MHz	
Dielectric constant				
water	ε'_w	$-0.2833 \times (T\text{-}273) + 80.67$		[39]
solid	ε'_s	Eq. (17)	–	[14]
gas	ε'_g	1	–	
Dielectric loss				
water	ε''_w	$0.05 \times T + 20$	–	[39]
solid	ε''_s	Eq. (18)	–	[14]
gas	ε''_g	0	–	
Transport				
Density				
water	ρ_w	998	kg/m^3	
vapor	ρ_v	Ideal gas	kg/m^3	
air	ρ_a	Ideal gas	kg/m^3	
solid	ρ_s	867.76	kg/m^3	This study
Specific heat capacity				
water	$C_{p,\,w}$	4176.2	J/kg K	[30]
vapor	$C_{p,\,v}$	2062	J/kg K	[30]
air	$C_{p,\,a}$	1006	J/kg K	[40]
solid	$C_{p,\,s}$	Eq. (19)	J/kg K	This study
Thermal conductivity				
water	k_w	0.57	W/m K	[40]
vapor	k_v	0.026	W/m K	[40]
air	k_a	0.026	W/m K	[40]
solid	k_s	Eq. (20)	W/m K	This study
Capillary diffusivity (water)	D_w	Eq. (24)	m^2/s	[41]
Constant in Antoine equation				
	A	7.8087		[42]
	B	1007.839	[K]	[42]
	C	−166.3583	[K]	[42]
Heat transfer coefficient	h_t	10	W/m^{2}K	[43]
Mass transfer coefficient	h_m	1×10^{-7}	m/s	[44]
Latent heat of evaporation	λ	9780	cal/mol	[34]
Evaporation rate constant	K_{vap}	1×10^{-6}	1/s	[32]
Porosity	φ	0.8		This study
Moisture expansion coefficient	β_h	0.672		[45]
Initial Conditions				
Water concentration	$c_{w,\,0}$	4094	mol/m^3	This study
Temperature	T_0	2 5	°C	This study
Moisture content (d.b.)	M_w	5.66	–	This study

with diameter 45.5 ± 5.4 mm. The initial moisture content and density of samples were listed in Table 1. The container (400 mm L × 270 mm W × 20 mm H) with twenty-four kiwifruit slices in four rows and six columns was placed at the center of the bottom electrode. The electrode gap of 60 mm and vacuum pressure of 0.02 MPa were selected to obtain suitable RF evaporation rate and stable temperature based on the experimental setup in the RF-vacuum drying [13]. Fiber-optic temperature sensors (HQ-FTS-D120, Heqi Technologies Inc., Xian, China) were inserted into the four kiwifruit slices in the geometric center of the container to record sample temperatures during the RF-vacuum drying process. Surface temperatures of kiwifruit slices were measured and analyzed using an infrared thermal imaging camera (FLIR A300, FLIR Systems, Stockholm, Sweden) having an accuracy of ±2 °C. Moisture content of kiwifruit slices was calculated by employing gravimetric method, supposing that the loss of weight in kiwifruit slices was caused by water evaporation during the RF-vacuum drying. Mass of samples was weighted by the electronic scale (AT8106, Pengheng Electronic Inc., Shanghai, China) and recorded every 10 min. The RF-vacuum drying system was turned off until the moisture content of sample was less than 0.13 kg/kg (d.b.). The detail information on RF-vacuum drying system and experimental process can be found in the previous study [13].

During RF-vacuum drying, water evaporated from kiwifruit samples with shrinkage and deformation phenomenon. The diameter and thickness of the sample were measured at three different locations using a digital caliper (DL91150, Deli Tools Co., Lt., Yuzhao, China). Therefore, the shrinkage was expressed by the ratio between the diameter or thickness of the sample after and before the RF-vacuum drying.

2.3. Sensitivity analysis of input parameters

A large number of input parameters are required for modeling the RF-vacuum drying of kiwifruit slices (Table 1). Some parameters could not be accurately and directly obtained from literatures, therefore, it is important to perform a sensitivity analysis to determine how these major parameters affect the drying process of kiwifruit slices. The sensitivity analysis was carried out for the four parameters, including capillary diffusivity values, evaporation rate constant, specific heat capacity and thermal conductivity values. Capillary diffusivity and evaporation rate constant values were varied by ±1000%, and specific heat capacity and thermal conductivity values were varied by ±50%, and their effect on temperature and moisture content, two of the most important drying properties associated with the sample were calculated.

2.4. Factors affecting the drying process

Several factors that affect the RF-vacuum drying have been identified, such as electrode gap of RF-vacuum system, thickness of kiwifruits slices, and vacuum pressure. Using the validated model developed above, the effect of electrode gap of 40, 50, 60, 70, and

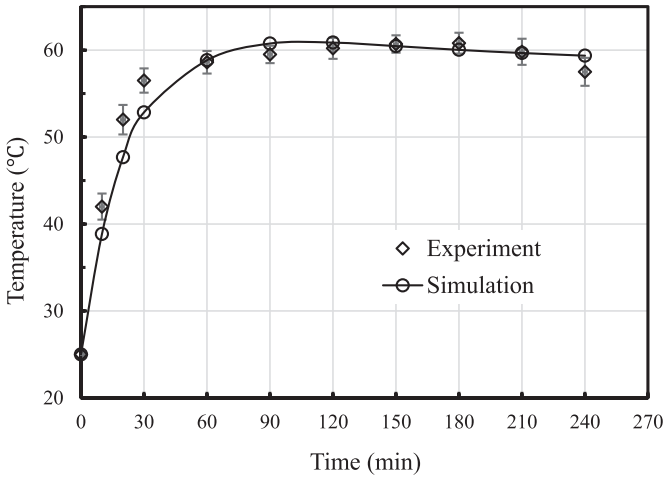

Fig. 2. Experimental [13] and simulated temperature-time histories near the center of the kiwifruit with the electrode gap of 60 mm and sample thickness of 8 mm under the vacuum pressure of 0.02 MPa during the RF-vacuum drying.

80 mm on the temperature and moisture content of samples with sample thickness 8 mm and vacuum pressure 0.02 MPa was discussed. Then, different thickness (4, 6, 8, 10, and 12 mm) of samples and vacuum pressures (0.01, 0.02, 0.03, and 0.04 MPa) were considered. Various factors were discussed to help understand the optimal conditions for the RF-vacuum drying.

2.5. Statistical analysis

Statistical analysis was conducted to determine the agreement between model and experimental values using relative percent error, which was estimated by the following equation [47]:

$$E(\%) = \frac{100}{\mathrm{n}} \sum_{i=1}^{n} \frac{\left|M_{\mathrm{exp},i} - M_{pre,i}\right|}{M_{\mathrm{exp},i}} \tag{25}$$

3. Results and discussion

The finite element model established was validated using experimental data from the previous study [13] and by comparing history of temperature, moisture content, and drying rate during RF-vacuum drying. The shrinkage and the factors affecting the drying process of kiwifruit slices were also discussed and followed by sensitivity analysis of input parameters affected the temperature and moisture content of samples.

3.1. Experimental validation

3.1.1. Temperature histories and distribution

Fig. 2 shows a comparison between the experimental and simulated temperatures at the center of the kiwifruit slices in the geometric center of the container during the RF-vacuum drying. There was a good agreement between the simulated temperatures and experimental results since the maximum relative error of temperature between the simulated values and the experimental results was less than 10%. At the beginning of RF-vacuum drying, the temperature of the kiwifruit slices with high moisture content, which absorbs more the RF energy and converts into heat, increased rapidly with time. The pressure and the evaporation rate of samples increased with increasing temperature, but the heating rate decreased. Therefore, the temperature-time history curve become smooth and continued to increase to a maximum value corresponding to the water boiling point (60 °C) under a vacuum pressure level of 0.02 MPa [48]. When the temperature reached the maximum value, the absorbed RF energy was mostly used for water evaporation. Then, decreases of moisture content in the kiwifruit slices again reduced the absorption of RF energy and thus the temperature gradually decreased [49]. At the end of drying, the sample temperature was slightly lower than 60 °C.

Fig. 3 shows a comparison between experimental and simulated temperature distributions of kiwifruit slices. Results demonstrated that the simulated temperature distribution pattern matched experimental one well. The highest temperature of kiwifruit slices after the RF-vacuum drying was 62.5 °C, which was located at corners while the lowest temperature was 59.5 °C and located at the center. The maximum temperature measured by experiment was higher than simulated value, but the lowest temperature was in reverse lower in experiments since heat loss of samples was observed during moving and measuring processes. The similar corners and edges effect, in which the sample temperature at corners and edges was higher than that in the sample center, was also found when chestnuts [24] and soybeans [50] were heated by RF energy. This can be explained by that electrical field intensity concentrated at corners and edges of the sample was higher than that in the center due to the electrical field refraction and reflection, and resulted in higher temperature distributions at corners and edges based on Eqs. (3) and (4) [24]. For a single kiwifruit slice, the cold spot location was found to be at the slice center based on both experimental and simulated results. Similar results were reported for peanut butter, which was packaged by a cylindrical container, when it was heated by RF energy [51].

3.1.2. Drying rate

Fig. 4 shows simulated and experimental drying rate/evaporation rate of samples during the RF-vacuum drying. At the beginning of RF-vacuum drying, the drying rate was zero due to the mass and energy balance. Then, the drying rate increased rapidly for the large temperature and pressure gradients according to Eq. (9) and reached a maximum value after about 40 min of RF heating. After the maximum value reached, the drying rate declined down sharply due to a decrease in temperature difference between the surface and the center and reduced rate of heat transfer. At the second half of drying process, the drying rate changed slowly and closed to zero because the lower moisture content reached under the vacuum conditions, almost all free water was evaporated from the sample, and the remaining bound water was removed. Similar behavior has been observed in microwave-vacuum dried kiwifruit drying [52].

3.1.3. Changing of moisture content

Fig. 5 shows a comparison between the simulated and experimentally observed moisture loss-time histories of the kiwifruit slices during the RF-vacuum drying. The simulated moisture content matched the experimental values well with maximum difference of less than 2%. The moisture content values decreased slowly during some initial minutes for the low temperature and low evaporation rate. Then, the moisture content values decreased rapidly when the sample temperature increased due to the temperature gradient between the kiwifruit slices and the surrounding, resulting in high evaporation rate. Due to the evaporation and moisture loss, the dielectric properties and gas porosity of samples decreased. According to Eq. (3), the RF energy absorption of samples would be lower due to lower dielectric properties, resulting in lower increase of temperatures and lower moisture loss. After 120 min of RF-vacuum drying, the moisture content of samples decreased from 5.66 to 0.67 (d.b.). Then the moisture content curve became flat at the later drying time and reached to 0.13 (d.b.) at the end of RF-vacuum drying.

Fig. 6 shows a simulated moisture content distribution of kiwifruit slices after the RF-vacuum drying. The highest moisture

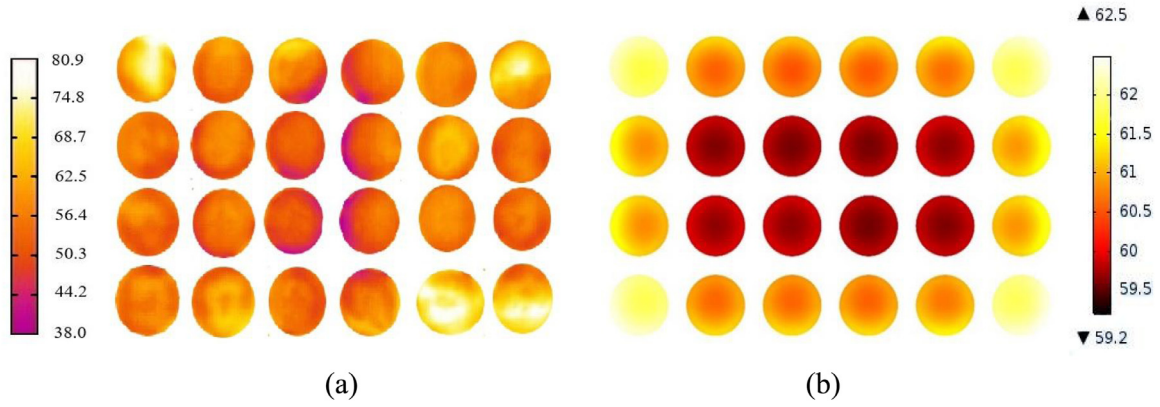

Fig. 3. Comparison of experimental (a) [13] and simulated (b) temperature (°C) distributions (top view) of kiwifruit placed on the bottom electrode with electrode gap of 60 mm and sample thickness of 8 mm under vacuum pressure of 0.02 MPa after the RF-vacuum drying.

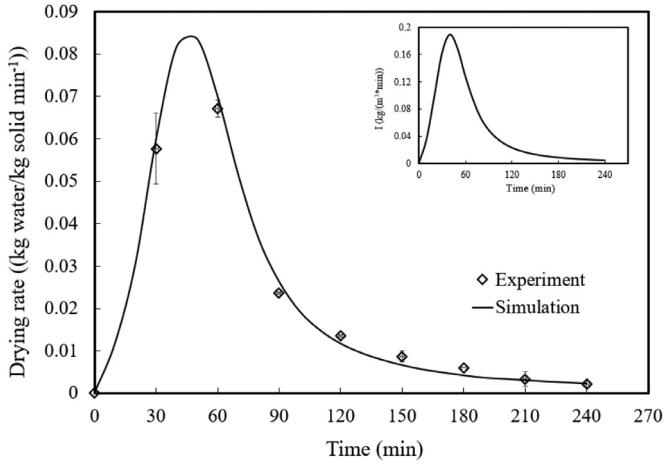

Fig. 4. Simulated and experimental [13] drying rate/evaporation rate (kg water/kg solid min^{-1}) near the center of the kiwifruit with the electrode gap of 60 mm and sample thickness of 8 mm under the vacuum pressure of 0.02 MPa during the RF-vacuum drying.

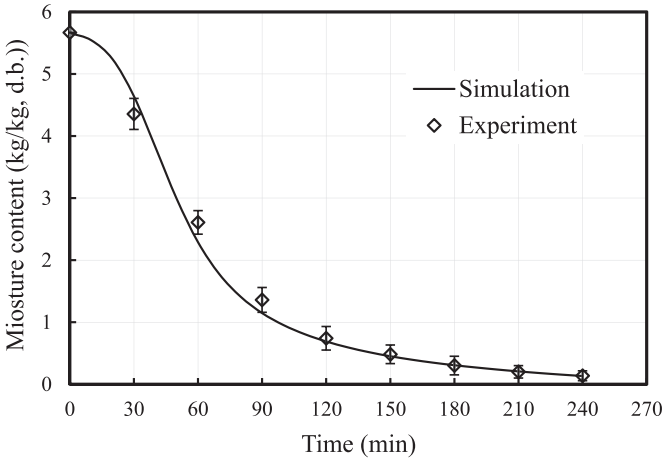

Fig. 5. Simulated and experimental [13] moisture loss (d.b.)-time histories of the kiwifruit slices with the electrode gap of 60 mm and sample thickness of 8 mm under the vacuum pressure of 0.02 MPa during the RF-vacuum drying.

content of samples after the RF-vacuum drying was located at the geometric center region of the container while the lowest moisture content was located at corners of the container. Fig. 7 shows simulated and experimental moisture contents at the central cross section of the kiwifruit slice located near the center of the container after the RF-vacuum drying, indicating that the lowest moisture content was located at the edge of slice and the highest one was located at the slice center. The distribution of moisture content in kiwifruit slices was opposite to that of temperature since the high temperature resulted in high evaporation rate, and low moisture content. The experimental moisture content (0.259 ± 0.013) at the center was higher than simulated values (0.188) but it (0.137 ± 0.005) was lower than simulated results (0.174) at the edge part although experimental and simulated moisture contents had the same average value. This result may be caused by central and edged parts of kiwifruit slice had different tissues and rehydration capacities.

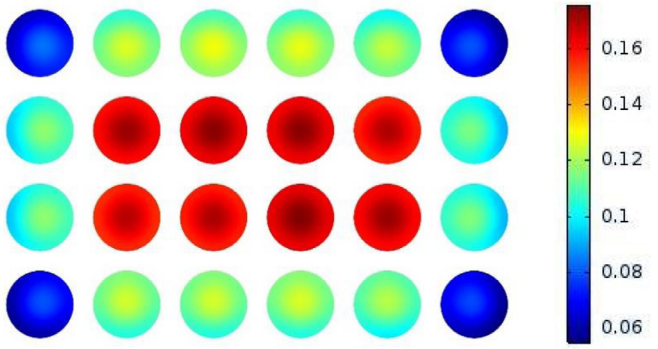

Fig. 6. Simulated moisture content (d.b.) (top view) of kiwifruit placed on the bottom electrode with the electrode gap of 60 mm and sample thickness of 8 mm under the vacuum pressure of 0.02 MPa after the RF-vacuum drying.

3.1.4. Shrinkage

Fig. 8 shows experimental and simulated shrinkages of the kiwifruit slice in the geometric center of the container during the RF-vacuum drying. After the drying process, long diameter, short diameter, and thickness of kiwifruit slices were 35.97 ± 1.68, 30.66 ± 1.34, and 3.70 ± 0.12 mm, respectively. Then, the shrinkage of kiwifruit slices were estimated to be 79.93%, 68.13%, and 46.25% for long axis, short axis, and thickness of kiwifruit slices, respectively. Obviously, the shrinkage of kiwifruit slices was nonuniform in the three directions. However, the shrinkage of kiwifruit slices was 72.52% by simulation based on the homogenous material. This result indicated that further research would be needed on the shrinkage and moisture content of kiwifruit slices using an accurate model to consider various tissues in different zone.

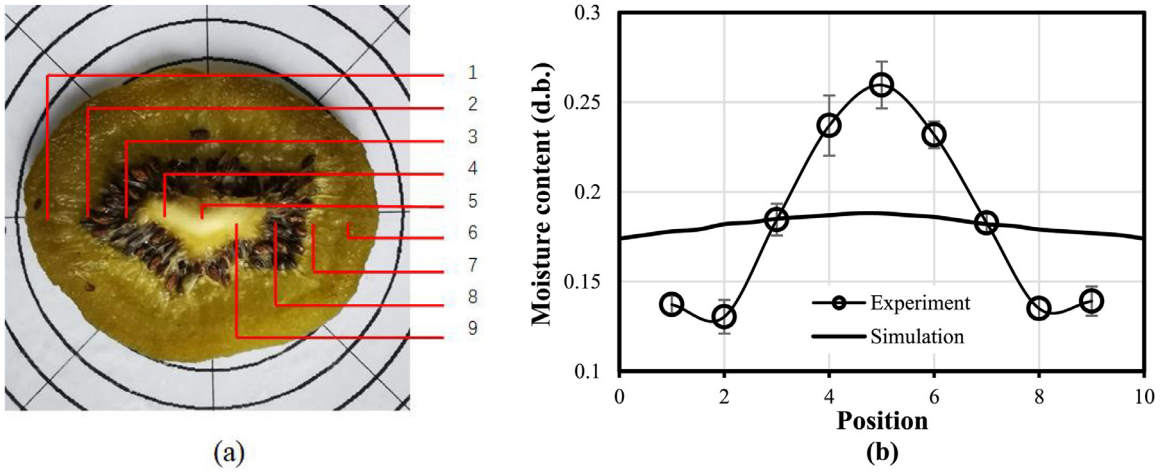

Fig. 7. Simulated and experimental [13] moisture contents (d.b.) at the central cross section of kiwifruit slice near the center of the container after the RF-vacuum drying (a. testing position, b. testing result).

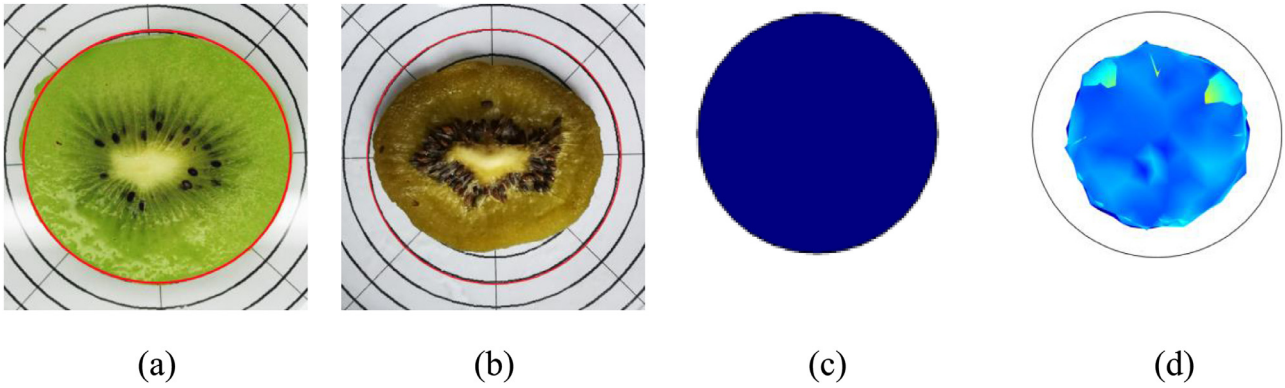

Fig. 8. Shrinkage of kiwifruit slices with the electrode gap of 60 mm and sample thickness of 8 mm under the vacuum pressure of 0.02 MPa before and after the RF-vacuum drying (a: experimental before drying, b: experimental after drying, c: simulated before drying, d: simulated after drying).

The above results indicated that the simulated temperature and moisture content profiles calculated by the established 3-D model matched experimental results well since the maximum relative error for temperature and moisture content was less than 10% and 2%, respectively. Furthermore, the simulated temperature and moisture content distribution pattern also matched experimental results well. Therefore, the validated model could be used to conduct a sensitivity analysis of input parameters and evaluate influences of the main factors on drying characteristics.

3.2. Sensitivity analysis

3.2.1. Capillary diffusivity

Since no experimentally measured value of capillary diffusivity for kiwifruit was found in the literature, a capillary diffusivity value was expressed by Eq. (24) for this model based on microwave drying of potato [41] and selected as a reference. Fig. 9 shows the calculated temperature- and moisture content-time histories of kiwifruit slices for two capillary diffusivity values, which were compared with the reference. When the capillary diffusivity value was higher or lower with ±1000% variations, no significant difference from the reference was observed for the temperature and moisture content of kiwifruit slices. Therefore, effect of different capillary diffusivity values on temperature and moisture content of samples during the RF-vacuum drying could be ignored based on the simulation results.

3.2.2. Evaporation rate constant

Experimentally measured value of evaporation rate constant of kiwifruit is not available in the literature. An evaporation rate constant of 10^{-6} 1/s used to simulate a vacuum drying of pharmaceutical compounds [32] was served as a reference. Fig. 10 shows the predicted temperature- and moisture content-time histories of kiwifruit slices as influenced by two values of evaporation rate constant and compared with the reference. According to Eq. (9), the higher evaporation rate constant resulted in higher evaporation rate. As a consequence, the temperature was slightly lower for the samples having higher evaporation rate constant while the moisture content of kiwifruit slices was obviously lower as compared with the reference. Therefore, the moisture content was more sensitive than the temperature to the changes of evaporation rate constant.

3.2.3. Specific heat capacity and thermal conductivity

Specific heat capacity and thermal conductivity values were calculated based on the major compositions of kiwifruit according to the method in the previous literature [37]. The calculated specific heat capacity and thermal conductivity values were used as the references. Figs. 11 and 12 show the calculated temperature- and moisture content-time histories of kiwifruit slices as influenced by two values of specific heat capacity and thermal conductivity, respectively, and compared with the references. The changes in specific heat capacity and thermal conductivity values in kiwifruit indicated very small changes in temperatures and moisture content values during the RF-vacuum drying. Therefore, more accurate val-

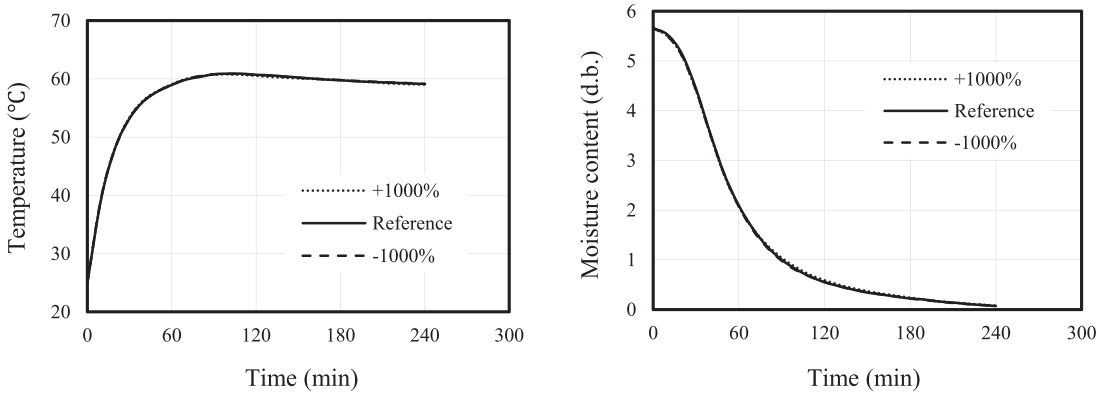

Fig. 9. Effect of capillary diffusivity on temperature (°C) (a) and moisture content (d.b.) (b) of kiwifruit slices with electrode gap of 60 mm and sample thickness of 8 mm under vacuum pressure of 0.02 MPa during the RF-vacuum drying.

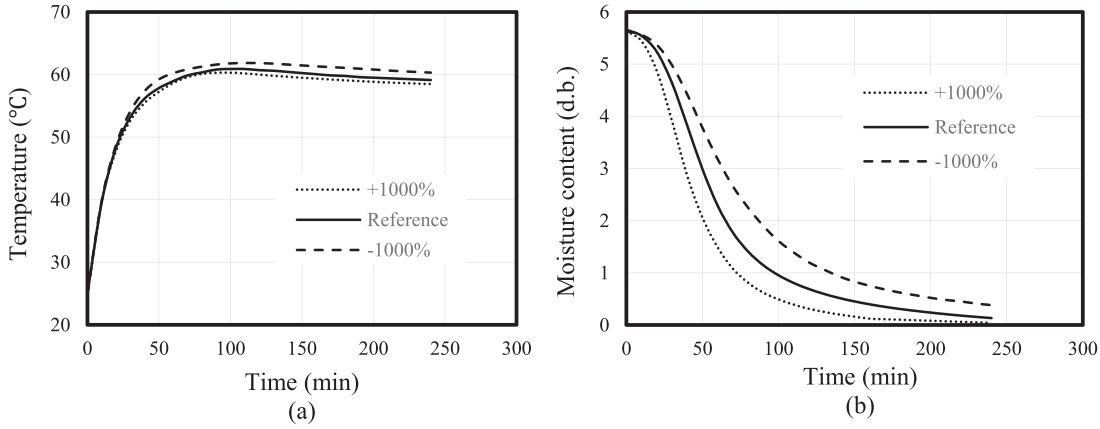

Fig. 10. Effect of evaporation rate constant on temperature (°C) (a) and moisture content (d.b.) (b) of kiwifruit slices with the electrode gap of 60 mm and sample thickness of 8 mm under the vacuum pressure of 0.02 MPa during the RF-vacuum drying.

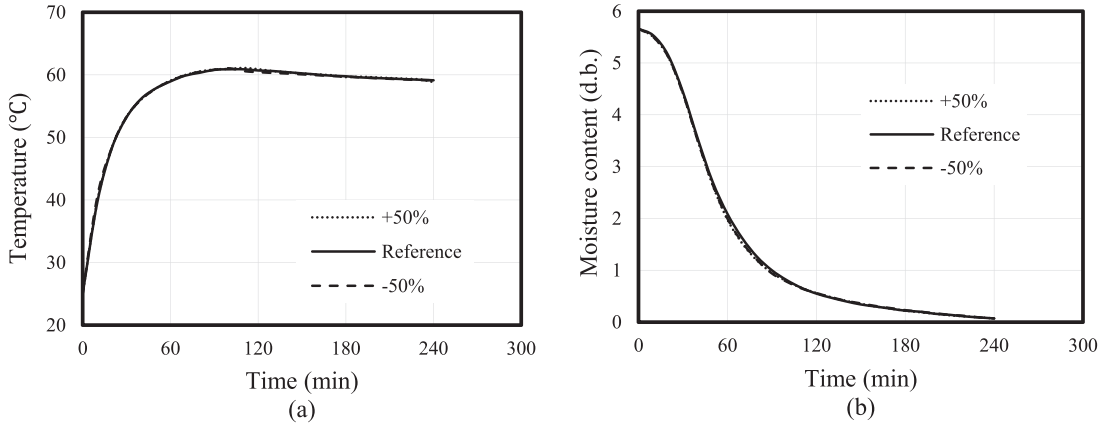

Fig. 11. Effect of specific heat capacity on temperature (°C) (a) and moisture content (d.b.) (b) of kiwifruit slices with the electrode gap of 60 mm and sample thickness of 8 mm under the vacuum pressure of 0.02 MPa during the RF-vacuum drying.

ues of specific heat capacity and thermal conductivity values might not be required for predicting the temperature or final moisture content of the kiwifruit slices during the RF-vacuum drying.

Four parameters, including capillary diffusivity values, evaporation rate constant, specific heat capacity and thermal conductivity values, were used for the sensitivity analysis. The moisture content was more sensitive than the temperature to the changes of evaporation rate constant. The changes in capillary diffusivity, specific heat capacity, and thermal conductivity values in kiwifruit resulted in very small changes in temperatures and moisture content values during the RF-vacuum drying. Therefore, more accurate values of capillary diffusivity, specific heat capacity, and thermal conductivity values might not be required for predicting moisture loss or final moisture content of the kiwifruit slices in this research.

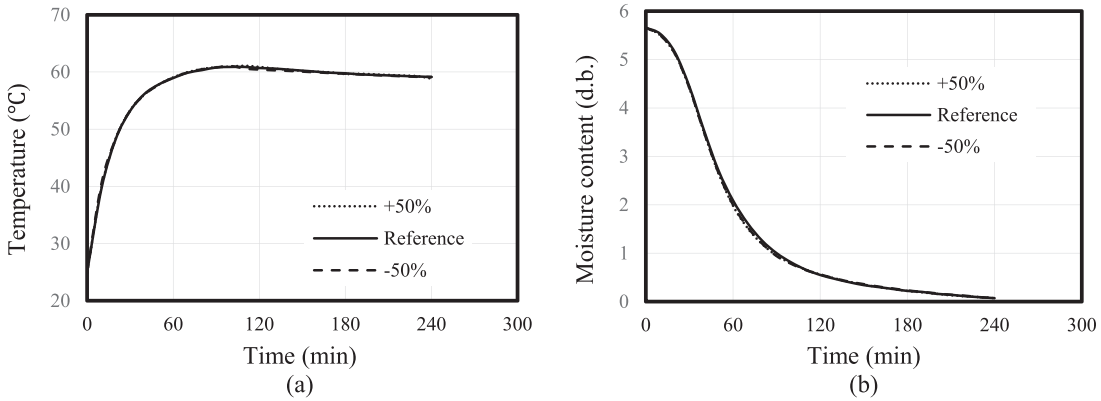

Fig. 12. Effect of thermal conductivity on temperature (°C) (a) and moisture content (d.b.) (b) of kiwifruit slices with the electrode gap of 60 mm and sample thickness of 8 mm under the vacuum pressure of 0.02 MPa during the RF-vacuum drying.

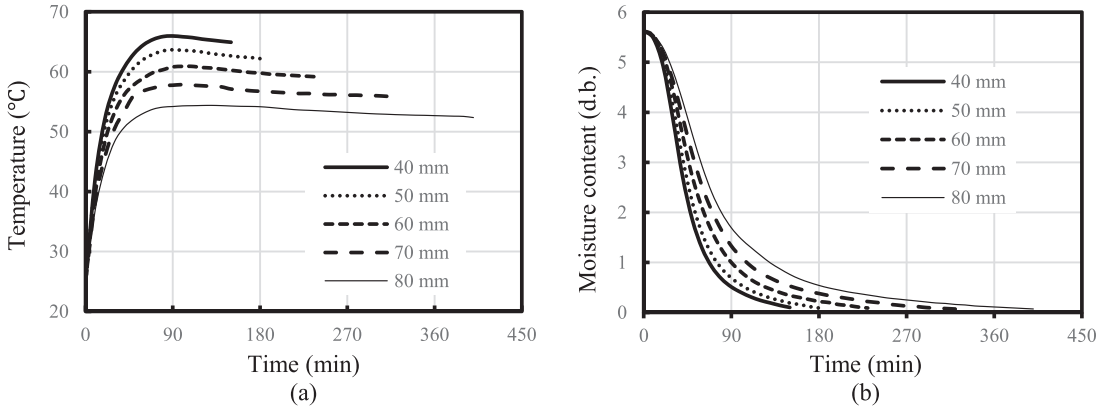

Fig. 13. Temperature (°C) (a) and moisture content (d.b.) (b) of kiwifruit slices with the electrode gaps of 40, 50, 60, 70, and 80 mm and sample thickness of 8 mm under the constant vacuum pressure of 0.02 MPa during the RF-vacuum drying.

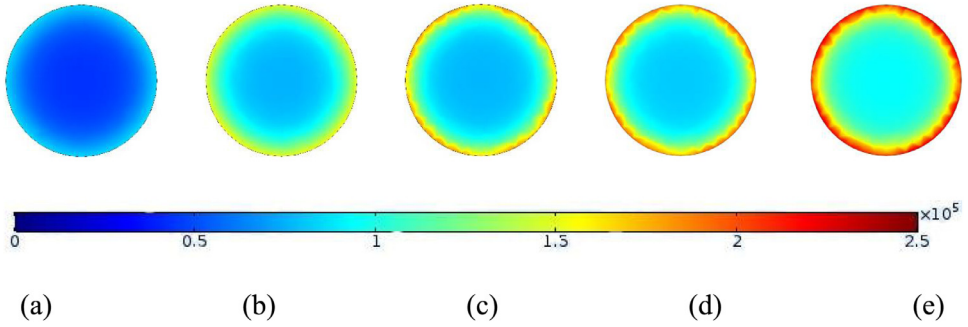

Fig. 14. Simulated electric field intensity (V/m) of kiwifruit slices in the geometric center region of the container with the sample thickness of 8 mm and different electrode gap (a. 80 mm, b. 70 mm, c. 60 mm, d. 50 mm, and e, 40 mm) under the vacuum pressure of 0.02 MPa during the RF-vacuum drying.

3.3. Factors affecting the drying process

3.3.1. Electrode gap of the RF-vacuum system

Fig. 13 shows the effect of electrode gap on temperature and moisture content of kiwifruit slices during the RF-vacuum drying. The total drying times required to reduce the moisture content of samples from 5.66 to 0.13 kg/kg (d.b.) were 140, 170, 200, 260, and 320 min for sample thickness of 8 mm and vacuum pressure of 0.02 MPa, and electrode gaps of 40, 50, 60, 70, and 80 mm, respectively (Fig. 13a). Based on Eqs. (2)–(4), the heating rates decreased with increasing electrode gap due to decreasing electric field intensity (Fig. 14). Furthermore, the electric field intensity of slice edge was obviously higher than that of the center, resulting in the corners and edges effect. The average sample temperatures at the different electrode gaps also increased gradually to their highest value during the RF heating and then remained relatively constant near the saturation temperature of water under the vacuum pressure of 0.02 MPa. While the sample temperature remained steadily, the drying rate increased rapidly and reached the peak value because the absorbed RF energy was mostly used for moisture evaporation. Generally, the smaller electrode gap resulted in higher RF heating-drying rates, but also resulted in some non-uniform heating and sometimes runaway heating occurred at the corners and edges of the samples.

3.3.2. Thickness of sample

The influences of kiwifruit slice thickness on RF-vacuum drying characteristics are shown in Fig. 15. In this study, the RF heat-

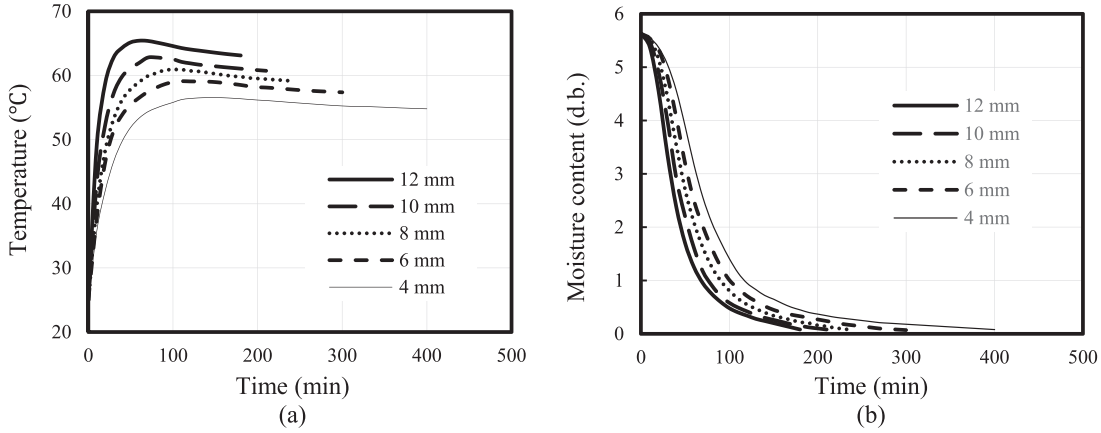

Fig. 15. Temperature (°C) (a) and moisture content (d.b.) (b) of kiwifruit slices with sample thickness of 12, 10, 8, 6, and 4 mm and the electrode gap of 60 mm under the constant vacuum pressure of 0.02 MPa during the RF-vacuum drying.

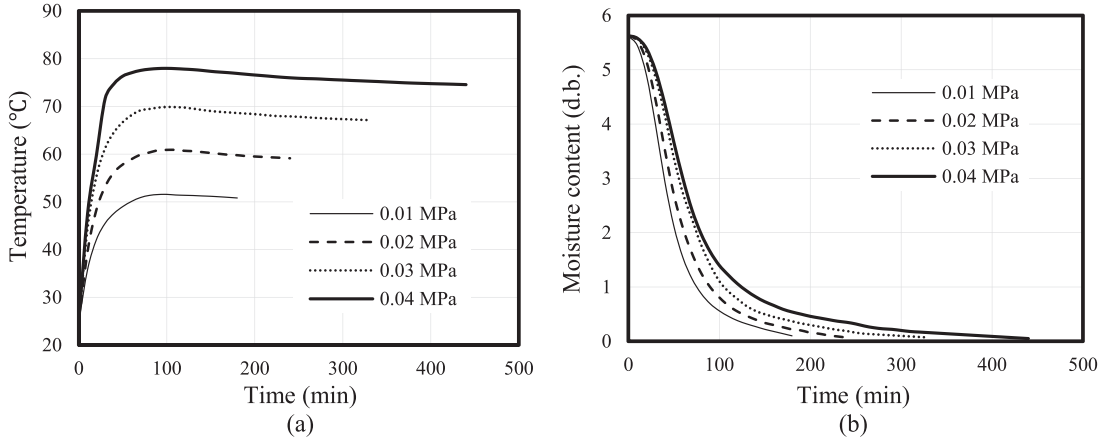

Fig. 16. Temperature (°C) (a) and moisture content (d.b.) (b) of kiwifruit slices with the constant electrode gap of 60 mm and sample thickness of 8 mm under the vacuum pressure of 0.01, 0.02, 0.03, and 0.04 MPa during the RF-vacuum drying.

ing rate of kiwifruit slices even increased with increasing sample thickness (Fig. 15a). This was because the air gap between top electrode and upper surface of sample simultaneously decreased with increasing sample thickness, resulting in more intense RF electric field distribution and faster heating rate [54]. When the sample thickness decreased from 12 to 4 mm, the RF-vacuum drying time increased from 160 to 310 min when the moisture content of samples decreased from 5.66 to 0.13 kg/kg (d.b.) at the tested electrode gap and vacuum pressure levels (60 mm gap and 0.02 MPa vacuum pressure) (Fig. 15b). However, the MW-vacuum drying time for kiwifruit slices was reported to increase from 14 to 24 min when sample thickness increased from 3 to 9 mm [53]. Although MW and RF treatments have similar heating mechanisms, the smaller penetration depth associated with MW as compared with RF heating is likely responsible for the slower heating rate associated with the former. Therefore, RF drying offers better advantages of heating/drying larger size or bulk materials as compared with MW drying.

3.3.3. *Vacuum pressure*

Fig. 16 shows the effect of different vacuum pressures (0.01, 0.02, 0.03, and 0.04 MPa) on RF-vacuum heating-drying characteristics with 60 mm electrode gap and 8 mm sample thickness. The heating rate and maximum temperature of sample increased with increasing vacuum pressure. This can be explained by the higher driving force of water vapor needed at lower pressure levels. Then less heat of evaporation could be necessary and resulted in higher water boiling point at lower pressure levels [52]. The results also suggested that RF-vacuum drying time decreased at lower vacuum pressure levels (higher vacuum). For example, the RF-vacuum drying time at the vacuum pressure of 0.04 MPa was 310 min, which was reduced to 160 min when the applied vacuum pressure was 0.01 MPa (Fig. 16b). The moisture diffusion rate was accelerated by lowering the vacuum pressure due to the high vapor pressure gradients. Similar results have also been reported for MW-vacuum drying of fruits/vegetables, such as apple slices [55], carrot slices [56], and lotus [57]. However, too low vacuum pressure may cause some potential technical problems in the RF-vacuum system.

The influences of three factors, including electrode gap, thickness of kiwifruit slices, and vacuum pressure, on RF-vacuum drying process were discussed. The temperature of kiwifruit slices increased with increasing thickness of kiwifruit slices, but decreasing electrode gap and vacuum pressure. But the drying time decreased with increasing thickness of kiwifruit slices, but decreasing electrode gap and vacuum pressure. Therefore, it is important to select appropriate electrode gap, thickness of kiwifruit slices, and vacuum pressure values to improve the RF drying efficiency. Based on above results, all the proposed aims of this simulation study were achieved.

4. Conclusions

In this study, a 3D model was developed to predict heat and mass transfer of kiwifruit during the RF-vacuum drying. Results

from computer simulation showed a good agreement with experimental values of the temperature, and moisture content of kiwifruit slices during the RF-vacuum drying and the validated model was used to conduct a sensitivity analysis of input parameters and evaluate influences of the main factors on drying characteristics. The temperature of the kiwifruit slices increased rapidly with time, reached the maximum value, and then gradually decreased. Furthermore, the drying rate increased rapidly at the begin of drying process and reached a maximum value after about 40 min of RF heating. At the second half of drying process, the drying rate changed slowly and closed to 0. Evaporation rate constant was found to be sensitive to moisture content of treated samples. The influences of thickness of kiwifruit slices, electrode gap, and vacuum pressure of the RF-vacuum system on temperature-, and moisture content-time history were investigated during the RF vacuum drying process. The temperature of kiwifruit slices increased with increasing thickness of kiwifruit slices, but decreasing electrode gap and vacuum pressure. While the drying time decreased with increasing thickness of kiwifruit slices, but decreasing electrode gap and vacuum pressure. The results in this study may provide useful information about this complicated drying process for further applications and optimizations.

Author statement

LH conducted simulation, analyzed data, and wrote the first version of manuscript. XZ helped to provide the experimental data and improved manuscript quality. SW is the PI of the project, guided the experimental design and revised manuscript.

Declaration of Competing Interest

We wish to confirm that there are no known conflicts of interest associated with this publication and there has been no significant financial support for this work that could have influenced its outcome. We confirm that the manuscript has been read and approved by all named authors and that there are no other persons who satisfied the criteria for authorship but are not listed. We further confirm that the order of authors listed in the manuscript has been approved by all of us. We confirm that we have given due consideration to the protection of intellectual property associated with this work and that there are no impediments to publication, including the timing of publication, with respect to intellectual property. In so doing we confirm that we have followed the regulations of our institutions concerning intellectual property.

Acknowledgments

This research was conducted in the College of Mechanical and Electronic Engineering, Northwest A&F University, and supported by research grants from National Key Research and Development Program of China (2018YFD0700105, 2017YFD0400900), Key Research and Development Program in Shaanxi Province of China (2018NY-105), and Open Fund from Key Laboratory of Northwest Agricultural Equipment (No. 2017NAE-2).

Supplementary materials

Supplementary material associated with this article can be found, in the online version, at doi:10.1016/j.ijheatmasstransfer.2020.119704.

References

[1] T. Ma, X. Sun, J. Zhao, Y. You, Y. Lei, G. Gao, J. Zhan, Nutrient compositions and antioxidant capacity of kiwifruit (Actinidia) and their relationship with flesh color and commercial value, Food Chem. 218 (2018) 294–304.
[2] T. Orikasa, S. Koide, S. Okamoto, T. Imaizumi, Y. Muramatsu, J. Takeda, T. Shiina, A. Tagawa, Impacts of hot air and vacuum drying on the quality attributes of kiwifruit slices, J. Food Eng. 125 (2014) 51–58.
[3] K. Ergün, G. Çalışkan, S.N. Dirim, Determination of the drying and rehydration kinetics of freeze dried kiwi (*Actinidia deliciosa*) slices, Heat Mass Transf. 52 (12) (2016) 2697–2705.
[4] M.V. Traffano-Schiffo, L. Laghi, M. Castro-Giraldez, U. Tylewicz, S. Romani, L. Ragni, M.D. Rosa, P.J. Fito, Osmotic dehydration of organic kiwifruit pre-treated by pulsed electric fields: internal transport and transformations analyzed by NMR, Innov. Food Sci. Emerg. Technol. 41 (2017) 259–266.
[5] A. Mustafa, K.M. Cagatay, Sliced kiwi drying in a solar energy and heat pump dryer, J. Fac. Eng. Archit. Gazi Univ. 28 (4) (2013) 733–741.
[6] Y. Wang, Y. Li, S. Wang, L. Zhang, M. Gao, J. Tang, Review of dielectric drying of foods and agricultural products, Int. J. Agr. Biol. Eng. 4 (1) (2011) 1–19.
[7] X. Zhou, S. Wang, Recent developments in radio frequency drying of food and agricultural products: a review, Drying Technol. 37 (3) (2019) 271–286.
[8] J. Hao, Y. Shen, L. Zhen, W. Li, Q. Zhang, Evaluation of strawberries dried by radio frequency energy, Drying Technol. 37 (3) (2019) 312–321.
[9] Y. Wang, L. Zhang, J. Johnson, M. Gao, J. Tang, J.R. Powers, S. Wang, Developing hot air-assisted radio frequency drying for in-shell macadamia nuts, Food Bioprocess Technol. 7 (1) (2014) 278–288.
[10] J. Peng, X. Yin, S. Jiao, K. Wei, K. Tu, L. Pan, Air jet impingement and hot air-assisted radio frequency hybrid drying of apple slices, LWT – Food Sci. Technol. 116 (2019) 108517.
[11] H. Zhang, C. Gong, X. Wang, M. Liao, J. Yue, S. Jiao, Application of hot air-assisted radio frequency as second stage drying method for mango slices, J. Food Process Eng. 42 (2) (2019) e12974.
[12] X. Zhou, H. Ramaswamy, Y. Qu, R. Xu, S. Wang, Combined radio frequency-vacuum and hot air drying of kiwifruits: effect on drying uniformity, energy efficiency and product quality, Innov. Food Sci. Emerg. Technol. 56 (2019) 102182.
[13] X. Zhou, R. Xu, B. Zhang, S. Pei, Q. Liu, H.S. Ramaswamy, S. Wang, Radio frequency-vacuum drying of kiwifruits: kinetics, uniformity, and product quality, Food Bioprocess Technol. 11 (11) (2018) 2094–2109.
[14] X. Zhou, R. Li, J.G. Lyng, S. Wang, Dielectric properties of kiwifruit associated with a combined radio frequency vacuum and osmotic drying, J. Food Eng. 239 (2018) 72–82.
[15] Z. Huang, F. Marra, J. Subbiah, S. Wang, Computer simulation for improving radio frequency (RF) heating uniformity of food products: a review, Crit. Rev. Food Sci. Nutr. 58 (6) (2018) 1033–1057.
[16] Z. Huang, F. Marra, Shaojin Wang, A novel strategy for improving radio frequency heating uniformity of dry food products using computational modelling, Innov. Food Sci. Emerg. Technol. 34 (2016) 100–111.
[17] Z. Huang, B. Zhang, F. Marra, Shaojin Wang, Computational modelling of the impact of polystyrene containers on radio frequency heating uniformity improvement for dried soybeans, Innov. Food Sci. Emerg. Technol. 33 (2016) 365–380.
[18] S. Zhang, Z. Huang, Shaojin Wang, Improvement of radio frequency (RF) heating uniformity for peanuts with a new strategy using computational modeling, Innov. Food Sci. Emerg. Technol. 41 (2017) 79–89.
[19] B. Alfaifi, J. Tang, Y. Jiao, S. Wang, B. Rasco, S. Jiao, S. Sablani, Radio frequency disinfestation treatments for dried fruit: model development and validation, J. Food Eng 120 (2014) 268–276.
[20] F. Marra, J. Lyng, V. Romano, B. McKenna, Radio-frequency heating of foodstuff: solution and validation of a mathematical model, J. Food Eng. 79 (3) (2007) 998–1006.
[21] Y. Jiao, H. Shi, J. Tang, F. Li, Shaojin Wang, Improvement of radio frequency (RF) heating uniformity on low moisture foods with polyetherimide (PEI) blocks, Food Res. Int. 74 (2015) 106–114.
[22] Q. He, C. Li, Modeling and simulation of the drying process of natural gas pipeline using vacuum drying method, Drying Technol. (2019) 1–12 in press.
[23] F. Nadi, D. Tzempelikos, Vacuum drying of apples (cv. golden delicious): drying characteristics, thermodynamic properties, and mass transfer parameters, Heat Mass Transf. 54 (7) (2018) 1853–1866.
[24] L. Hou, Z. Huang, X. Kou, S. Wang, Computer simulation model development and validation of radio frequency heating for bulk chestnuts based on single particle approach, Food Bioprod. Process. 100 (Part A) (2016) 372–381.
[25] B. Alfaifi, J. Tang, B. Rasco, S. Wang, S. Sablani, Computer simulation analyses to improve radio frequency (RF) heating uniformity in dried fruits for insect control, Innov. Food Sci. Emerg. Technol. 37 (2016) 25–137.
[26] S.L. Birla, S. Wang, J. Tang, Computer simulation of radio frequency heating of model fruit immersed in water, J. Food Eng 84 (2) (2008) 270–280.
[27] C.M.T. Choi, Finite element modeling of the rf heating process,, IEEE Trans. Magn. 27 (5) (1991) 4227–4230.
[28] R. Uyar, T.F. Bedane, F. Erdogdu, T.K. Palazoglu, K.W. Farag, F. Marra, Radio-frequency thawing of food products – a computational study, J. Food Eng 146 (2015) 163–171.
[29] V. Karageorgiou, D. Kaplan, Porosity of 3D biomaterial scaffolds and osteogenesis, Biomaterials 26 (27) (2005) 5474–5491.
[30] H. Zhu, T. Gulati, A.K. Datta, K. Huang, Microwave drying of spheres: coupled electromagnetics-multiphase transport modeling with experimentation. part I: model developmentand experimental methodology, Food Bioprod. Process. 96 (2015) 314–325.
[31] T. Stocker, Introduction to Climate Modelling, Springer, Berlin, Heidelberg, 2011.
[32] M. Murru, Giovanni Giorgio, Sara Montomoli, Francois Ricard, Fran-

tisek Stepanek, Model-based scale-up of vacuum contact drying of pharmaceutical compounds, Chem. Eng. Sci. 66 (21) (2011) 5045–5054.
[33] H.R. Kemme, S.I. Kreps, Vapor pressure of primary n-alkyl chlorides and alcohols, J. Chem. Eng. Data 14 (1) (1969) 98–102.
[34] I.M. Smallwood, Handbook of Organic Solvent Properties, Elsevier, Amsterdam, 1996.
[35] J. Delgado, Heat and Mass Transfer in Porous media, Advanced Structured Materials, Springer, Berlin, Heidelberg, 2011.
[36] R. Kessentini, O. Klinkova, I. Tawfiq, M. Haddar, Modeling the moisture diffusion and hygroscopic swelling of a textile reinforced conveyor belt, Polym. Test. 75 (2019) 159–166.
[37] S. Sahin, S.G. Sumnu, Physical Properties of Food, Springer, New York, 2006.
[38] D. Castaldo, V.A. Lo, A. Trifiro, S. Gherardi, Composition of Italian kiwi (Actinidia chinensis) puree, J. Agr. Food Chem. 40 (4) (1992) 594–598.
[39] S.O. Nelson, A.K. Datta, Handbook of Microwave Technology for Food Applications, Marcel Dekker, New York, 2001.
[40] Y. Choi, Okos, Effects of temperature and composition on the thermal properties of foods, J. Food Process Appl. 1 (1986) 93–101.
[41] A. Halder, A. Dhall, A.K. Datta, An improved, easily implementable, porous media based model for deep-fat frying: part I: model development and input parameters, Food Bioprod. Process. 85 (3) (2007) 209–219.
[42] G. Thomson, The antoine equation for vapor-pressure data, Chem. Rev. 38 (1) (1946) 1–39.
[43] V. Rakesh, A.K. Datta, Microwave puffing: determination of optimal conditions using a coupled multiphase porous media – large deformation model, J. Food Eng. 107 (2) (2011) 152–163.
[44] R.P.F. Guine, M.F.S. Brito, J.R.P. Ribeiro, Evaluation of mass transfer properties in convective drying of kiwi and eggplant, Int. J. Food Eng. 13 (7) (2017) 20160257.
[45] Y. Yuan, L. Tan, Y. Xu, Y. Yuan, J. Dong, Numerical and experimental study on drying shrinkage-deformation of apple slices during process of heat-mass transfer, Int. J. Therm. Sci. 136 (2019) 529–548.
[46] J. Chen, K. Pitchai, S. Birla, D. Jones, M. Negahban, J. Subbiah, Modeling heat and mass transport during microwave heating of frozen food rotating on a turntable, Food Bioprod. Process. 99 (2016) 116–127.
[47] J. Aprajeeta, R. Gopirajah, C. Anandharamakrishnan, Shrinkage and porosity effects on heat and mass transfer during potato drying, J. Food Eng. 144 (2015) 119–128.
[48] R.C. Rodgers, G.E. Hill, Equations for vapour pressure versus temperature: derivation and use of the antione equation on hand-held programmable calculator, Brit. J. Anaesth. 50 (5) (1978) 415–424.
[49] M. Natt, V. Somsak, R. Phadungsak, An experimental study of microwave drying under low pressure to accelerate the curing of Portland cement pastes using a combined unsymmetrical double-fed microwave and vacuum system, Int. J. Heat Mass Transf. 127 (2018) 179–192.
[50] Z. Huang, L. Chen, S. Wang, Computer simulation of radio frequency selective heating of insects in soybeans, Int. J. Heat Mass Transf. 90 (2015) 406–417.
[51] Y. Jiao, J. Tang, S. Wang, A new strategy to improve heating uniformity of low moisture foods in radio frequency treatment for pathogen control, J. Food Eng. 141 (2014) 128–138.
[52] S. Ambros, P. Foerst, U. Kulozik, Temperature-controlled microwave-vacuum drying of lactic acid bacteria: impact of drying conditions on process and product characteristics, J. Food Eng. 224 (2018) 80–87.
[53] H. Darvishi, P. Mohammadi, M. Azadbakht, Z. Farhudi, Effect of different drying conditions on the mass transfer characteristics of kiwi slices, J. Agr. Sci. Technol. 20 (2) (2018) 249–264.
[54] G. Tiwari, S. Wang, J. Tang, S.L. Birla, Analysis of radio frequency (RF) power distribution in dry food materials, J. Food Eng. 104 (4) (2011) 548–556.
[55] Q. Han, L. Yin, S. Li, B. Yang, J. Ma, Optimization of process parameters for microwave vacuum drying of apple slices using response surface method, Drying Technol. 28 (4) (2010) 523–532.
[56] Z. Cui, S. Xu, D. Sun, Microwave-vacuum drying kinetics of carrot slices, J. Food Eng. 65 (2) (2004) 157–164.
[57] Y. Tian, Y. Zhang, S. Zeng, Y. Zheng, F. Chen, Z. Guo, Y. Lin, B. Zheng, Optimization of microwave vacuum drying of lotus (*Nelumbo nucifera* gaertn.) seeds by response surface methodology, Food Sci. Technol. Int. 18 (5) (2012) 477–488.